Published in final edited form as:
Int J Radiat Oncol Biol Phys. 2014 October 1; 90(2): 446–453. doi:10.1016/j.ijrobp.2014.06.015.

Toward Distinguishing Recurrent Tumor from Radiation Necrosis: DWI and MTC in a Gamma Knife® Irradiated Mouse Glioma Model

Carlos J Perez-Torres, PhD[1], **John A Engelbach, AS**[1], **Jeremy Cates, PhD**[2], **Dinesh Thotala, PhD**[2], **Liya Yuan, PhD**[3], **Robert E Schmidt, MD, PhD**[5], **Keith M Rich, MD**[2,3], **Robert E Drzymala, PhD**[2], **Joseph JH Ackerman, PhD**[1,4,5], and **Joel R Garbow, PhD**[1,*]

[1]Department of Radiology, Washington University, Saint Louis, Missouri, United States

[2]Department of Radiation Oncology, Washington University, Saint Louis, Missouri, United States

[3]Department of Neurosurgery, Washington University, Saint Louis, Missouri, United States

[4]Department of Chemistry, Washington University, Saint Louis, Missouri, United States

[5]Department of Neuropathology, Washington University, Saint Louis, Missouri, United States

[6]Department of Internal Medicine, Washington University, Saint Louis, Missouri, United States

Abstract

Purpose—Accurate non-invasive diagnosis is vital for effective treatment planning. Presently, standard anatomical MRI is incapable of differentiating recurring tumor from delayed radiation injury, as both lesions are hyperintense in both post-contrast T1- and T2-weighted images. Further studies are therefore necessary to identify an MRI paradigm that can differentially diagnose these pathologies. Mouse glioma and radiation injury models provide a powerful platform for this purpose.

Methods and Materials—Two MRI contrasts that are widely employed in the clinic were chosen for application with a glioma/radiation-injury model: diffusion weighted imaging, from which the apparent diffusion coefficient (ADC) is obtained, and magnetization transfer contrast, from which the magnetization transfer ratio (MTR) is obtained. These metrics were evaluated longitudinally, first in each lesion type alone – glioma vs. irradiation - and then in a combined irradiated glioma model.

Results—MTR was found to be consistently decreased in all lesions compared to nonlesion brain tissue (contralateral hemisphere), with limited specificity between lesion types. In contrast, ADC, though less sensitive to the presence of pathology, was increased in radiation injury and decreased

*Corresponding Author: Joel R Garbow Biomedical MR Laboratory Campus Box 8227 Washington University School of Medicine Room 2313, 4525 Scott Ave, St Louis, MO 63110, USA Fax: +1 314 362 0526 Phone: +1 314 362 9949 garbow@wustl.edu.

Conflict of Interest: None

in tumors. In the irradiated glioma model, ADC also increased immediately after irradiation, but decreased as the tumor regrew.

Conclusions—ADC is a better metric than MTR for differentiating glioma from radiation injury. However, MTR was more sensitive to both tumor and radiation injury than ADC, suggesting a possible role in detecting lesions that do not enhance strongly on T1-weighted images.

Keywords

Glioma; Radiation; Magnetization Transfer; Diffusion Weighted Imaging

Introduction

The standard approach for the treatment of glioma is a combination of surgery, radiotherapy, and chemotherapy (1-3). Like any other treatment, there are side effects associated with the radiotherapy treatment regimen. Delayed radiation injury, also known as radiation necrosis, is a serious complication seen in up to 23% of patients (4) that can occur months to years after radiotherapy. A major challenge in evaluating brain tumor patients treated with radiation is that radiation injury can be confused easily with tumor progression in standard neuroimaging tests (5-8) and produces similar clinical symptoms.

The pathology of radiation necrosis includes hemorrhage, edema, neuronal cell death, demyelination, and endothelial cell death leading to blood brain barrier (BBB) breakdown (9-12). BBB breakdown, in turn, leads to increased signal in post-contrast T1-weighted imaging, while edema leads to increased signal in T2-weighted imaging. However, both of these imaging features are common to tumors, like glioma, as well. Pathologically, an obvious difference between tumor and radiation injury is that the former has high proliferation, and therefore high cellularity, while the latter has high cell death, and therefore low cellularity.

The standard magnetic resonance imaging (MRI) approach for investigating changes in cellularity is diffusion weighted imaging (DWI). The primary metric derived from DWI is the apparent diffusion coefficient (ADC), which reflects the barriers and restrictions imposed by cell walls and subcellular structures on the incoherent displacement motion of water. In tumors, ADC is negatively correlated with proliferation (13-15) and cellularity (16-18). Another MRI approach that can be used to investigate cellularity is magnetization transfer contrast (MTC). The primary metric derived from MTC is the magnetization transfer ratio (MTR), which reflects the macromolecular content of tissue. In tumor, MTR has been shown to be positively correlated with tumor grade (19,20) and cellularity (21). Thus, ADC and MTR probe tissue cellularity in a complementary fashion, with the former reflecting tissue organization and the latter reflecting primarily macromolecular content.

Our group has recently developed an animal model of focal delayed radiation injury that recapitulates the histological progression seen in patients and has characterized this model *via* anatomical T1- and T2-weighted MRI (22, 23). Herein, this focal delayed radiation injury model is combined with a well-validated intracerebral glioma model utilizing the

murine astrocytoma DBT cell line (24,25). Since the cell line is murine in origin, immunocompetent mice can advantageously be employed to generate a more accurate and complete representation of the irradiated glioma model. MTR and ADC were evaluated as potential biomarkers of cellularity in the irradiated glioma model as well as the late-onset radiation injury and glioma models individually. Of particular interest was the potential of MTR and ADC to distinguish between the two pathologies, to monitor their evolution over time, and to characterize therapeutic response.

Methods and Materials

Mouse Models

All experiments were approved by the institute's Division of Comparative Medicine and were performed on 8-9 week old female BALB/c mice (Harlan Laboratories, Indianapolis, IN). For the delayed radiation injury model (N=7), mice received an intraperitoneal injection of ketamine/xylazine anesthetic and were then restrained in custom-made holder that attaches to the stereotactic frame of the Leksell Gamma Knife Perfexion (Elekta, Stockholm, Sweden). A single, 50 Gy radiation dose (50% isodose) was focused on the cortex of the left hemisphere ~ 3 mm posterior to bregma. For the glioma model (N=10), mice were secured in a stereotactic frame and anesthetized with isoflurane. DBT cells (24) (~10,000 in 10 μl) were implanted over 3 minutes at a site 1 mm anterior and 2 mm to the left of bregma and 2 mm below the cortical surface. For the irradiated glioma model (N=10), tumors were similarly implanted and tumor size and location were confirmed at post-implantation day (PImD) 10. Mice then received three Gamma Knife radiation treatments of 7.5 Gy each (50% isodose) on PImD 10, 12, and 14, for a total radiation dose of 22.5 Gy. For both irradiated and non-irradiated tumor models, mice were imaged every three days until they were sacrificed or died due to disease progression. Mice were sacrificed if they lost more than 20% bodyweight or suffered obvious behavioral detriments (e.g., ataxia). After sacrificing, heads were removed and fixed in formaldehyde, after which brains were extracted and processed for paraffin sectioning and subsequent hematoxylin and eosin (H&E) staining.

Magnetic Resonance Imaging

Mice were anesthetized with isoflurane and restrained in a 3-point head holder. Images were acquired with a 4.7 T small-animal Agilent/Varian DirectDrive1 scanner using an actively decoupled volume coil (transmit) and 1.5 cm surface coil (receive). Before loading into the magnet, mice were given an intraperitoneal injection of 0.5 mL MultiHance (gadobenate dimeglumine, Bracco Diagnostics Inc, Princeton, NJ) contrast agent diluted 1:10 in sterile saline. Several datasets were acquired for each animal, including: MTC, DWI, and anatomical post-contrast T1-weighted. With the exception of DWI, all data were collected with a field of view of 15×15 mm^2 and 21 contiguous slices with a thickness of 0.5 mm. For DWI, only 11 contiguous slices were acquired, chosen to exactly match slices acquired with the other methodologies. For MTC analysis, proton-density-weighted images were acquired with and without the application of a 10 ms, 500° saturation pulse applied at a frequency offset +10 ppm from the water resonance. The MTR was calculated as the percent signal lost due to the saturation pulse: MTR = (Off - On) / Off. For DWI analysis, the

isotropic apparent diffusion coefficient (ADC) was calculated as the average of three separate diffusion datasets, acquired with diffusion encoding along 3 orthogonal directions, with a b-value of 1000 s/mm^2, plus a reference dataset with a b-value of 0.

Data Analysis and Statistics

Datasets were analyzed using custom-written Matlab software (The Mathworks, Natick MA), where regions of interest (ROI) for the contralateral and ipsilateral hemispheres were drawn manually on the post-contrast T1-weighted image. The extent of the T1-enhancing lesion was determined *via* a threshold segmentation algorithm within whole-brain (contralateral plus ipsilateral hemisphere) ROIs. To compensate for the inhomogeneity of the surface coil, the threshold segmentation was performed on a normalized T1 image generated by dividing the T1-weighted image by the MTC reference image (itself a proton-density-weighted image). Since both images suffer equivalently from the surface coil inhomogeneity, this normalization cancels out the inhomogeneity and enhances the T1 contrast. MTR and ADC maps were calculated in a voxel-by-voxel fashion and the ROIs were then applied to the resulting parametric maps. The median value for each metric across each ROI was calculated for comparison between groups. Graphs and statistical analyses were conducted on the region-based calculations with Prism (GraphPad Software, San Diego, CA). All graphs show mean and standard deviation for each group. Repeated Measures Two-Way ANOVA with Bonferroni post-tests were used for the statistical analysis to match each lesion ROI to its corresponding contralateral ROI or to match the specific MTR and ADC ratios for each animal.

Results

ADC is elevated and MTR is lowered in delayed radiation injury

Mice (N=7) were given a single 50 Gy radiation treatment and then underwent MRI examination from 1 to 12 weeks post-irradiation (8 time points). Representative parametric maps for all metrics at selected time points are shown in **Figure 1A** and for all time points in **Supplementary Figure 1**. As would be expected from a delayed injury model, and consistent with prior work (22, 23), there is no identifiable damage until at least 3-4 weeks post irradiation. Qualitatively, it was not possible to identify areas of damage in either the MTR or ADC maps before the lesion was visible in the post-contrast T1-weighted image.

The lesion ROI was defined in each mouse across multiple slices based solely on the enhancement in the post-contrast T1-weighted image. An ROI drawn in the contralateral hemisphere served as control. These ROIs were applied to the MTR and ADC maps to calculate the MTR and ADC for each ROI at each time point and the values are shown in **Figure 1B**. Compared to the contralateral hemisphere, the MTR value was consistently lower in the lesion and dropped further in value as the lesion progressed. At week 4 post-irradiation the MTR for the lesion was 0.57, while for the contralateral hemisphere it was 0.64. By week 12 post-irradiation, the MTR for the lesion had dropped to 0.37, while for the contralateral hemisphere it was 0.63 ($P<0.001$ for weeks 4 to 12 PIR). In this regard, the MTR was quite sensitive to the appearance of the lesion. In contrast, at early time points, the ADC was not significantly different from the contralateral hemisphere, but became

significantly elevated in value at later time points as the lesion progressed. At week 4 post-irradiation, the ADC for the lesion was 0.70 μm^2/ms, while for the contralateral hemisphere it was 0.72 μm^2/ms ($P>0.05$). By week 12 post-irradiation, the ADC for the lesion had increased to 1.13, while for the contralateral hemisphere it was 0.79 ($P<0.001$).

Both ADC and MTR are decreased in the glioma model

As with the radiation injury model, an orthotopic glioma model generated by implanting murine DBT cells subcortically was evaluated. Mice (N=10) were imaged on PImD 10 and then, subsequently, every three days until they were sacrificed. The implanted tumors have a diffuse appearance in post-contrast T1-weighted images. The primary endpoint that defined when each mouse was sacrificed was 20% weight loss. Representative maps for all metrics at selected time points are shown in **Figure 2A**.

ROIs were drawn in the same manner as for the radiation injury model, and MTR and ADC were calculated for each ROI at each time point as shown in **Figure 2B**. The MTR value was consistently lower in the tumor in comparison to the contralateral hemisphere. At all time points the MTR for the lesion was between 0.49 and 0.51, while for the contralateral hemisphere it was between 0.62 and 0.64 ($P<0.001$ for all time points). ADC was not as sensitive as the MTR at the early time points; however, the ADC dropped progressively in value as the tumor grew. At PImD 10, the ADC for the lesion was 0.76 μm^2/ms, while for the contralateral hemisphere it was 0.78 μm^2/ms ($P>0.05$). By PImD 19, the ADC for the lesion had decreased to 0.63, while for the contralateral hemisphere it was 0.75 ($P<0.001$).

ADC can differentiate glioma from radiation injury while MTR cannot

Figure 3 includes early and late time data for both radiation injury and tumor. Consistent with previous findings, MTR at the late radiation injury time point is significantly lower than at the early radiation time point or in tumor. MTR is also significantly lower in late-stage tumors compared with early radiation injury. Given that the MTR for late-stage tumor is intermediate to that of early tumor and late radiation injury, it would be difficult to differentiate radiation injury from tumor based on MTR alone. In contrast, the ADC for late radiation injury is significantly higher than for either early radiation injury or tumor. At the same time, the ADC of the late tumor is significantly lower than that of both early tumor and early and late radiation injury. Since the ADC change in tumor is opposite in direction to that in radiation injury, it is possible to use ADC to differentiate between these pathologies.

ADC is temporarily elevated after irradiation of the glioma model

Having separately characterized both radiation injury in brain tissue and tumor, an irradiated glioma model was also examined. DBT glioma cells were implanted in mice (N=10), as described previously, and tumor growth and location were confirmed on PImD 10 prior to the start of radiation treatment. Mice having tumors that were not completely confined to the left hemisphere were excluded from the study. MTR and ADC maps at this PImD 10 time point precede irradiation and match those of the nonirradiated glioma model described earlier (**Figure 2)**. Mice received three irradiation treatments of 7.5 Gy each on PImD 10, 12 and 14, for a total radiation dose of 22.5 Gy. While this dose of radiation was not curative, it was enough to significantly increase the survival time after tumor implantation with a

median survival of 27.5 days for irradiated versus 19 days for non-irradiated for a P=0.001 by Log-rank (Mantel-Cox) Test, as shown in **Supplementary Figure 2**.

Mice with irradiated tumors present with heterogeneous lesions, as illustrated in **Figure 4A**. MTR and ADC were again calculated for the same ROIs as before and are shown in **Figure 4B**. Consistent with **Figure 3** and all previous data, MTR was consistently lower in the irradiated tumor in comparison to the contralateral hemisphere. However, ADC was elevated immediately following treatment, before eventually reverting to a value comparable to that of the contralateral hemisphere. At PImD 10, before irradiation, the MTR and ADC values were similar to the glioma model with the lesion having an MTR of 0.47 and ADC of 0.71 μm^2/ms and the contralateral hemisphere having an MTR of 0.62 and ADC of 0.73 μm^2/ms ($P<0.001$ for MTR and $P>0.05$ for ADC). The MTR was consistently lower in the lesion before and after irradiation and for the most part remained stable ranging from 0.47 to 0.54 in the lesion, while the contralateral hemisphere ranged from 0.61 to 0.64. In contrast, by PImD 20, the ADC in the lesion had risen to 0.82 μm^2/ms, while the contralateral hemisphere was at 0.75 μm^2/ms ($P<0.001$). This increase was only temporary and by PImD 29 the ADC in the lesion was 0.78 μm^2/ms, while the contralateral hemisphere was at 0.75 μm^2/ms ($P>0.05$). Based on the results shown in **Figure 3**, the increase in ADC likely reflects areas of dead tumor tissue resulting from the radiation treatment.

MRI data and H&E histology findings are consistent

Figure 5 presents example MRI data and correlative histology at the final time point from the tumor (middle panels), radiation (top), and irradiated tumor (bottom) groups. The irradiated tumor was variable at the final time point so **Figure 5** presents a case that had a clear mixed ADC phenotype.

Discussion

Given the prevalence of radiation therapy in the treatment of brain tumors, be they gliomas or metastatic lesions, differentiation of recurrent tumor from delayed radiation injury is a major unmet challenge. Multiple groups have attempted to address this challenge through various imaging approaches targeting fundamental differences between the pathologies. Specifically, researchers have looked at differences in blood flow and perfusion (26-28), metabolism (28-30), and cellularity and tissue composition (30-32). The work presented herein is distinct from prior studies in that the Leskel Gamma Knife mouse irradiation model is a single hemisphere model of radiation injury that recapitulates all of the histologic hallmarks of the clinical lesion (22, 23) while allowing use of the unaffected hemisphere as a valuable control within each subject, data were acquired at multiple times during progression of the injury models, and results are presented for a combined irradiated glioma model, rather than solely for each pathology alone. While the images in **Figures 1**, **2**, and **4** show only single slices, all metrics were averages, computed for multiple slices covering the entire lesion.

Because our study was designed to track the MRI metrics longitudinally for each mouse subject throughout the whole time course of lesion progression, it was not possible to obtain correlative histology at each time point. **Figure 5** presents example MRI data and correlative

histology at the final time point for a case of the irradiated tumor that had a clear mixed ADC phenotype. In this case, the H&E staining shows necrotic tumor within live tumor providing further support that ADC can identify live versus dead tumor. **Figure 5** also illustrates some of the challenges in discriminating between tumor and radiation injury as the T1-weighted image and MTR map would not be conclusive in separating these groups even though the H&E staining t is completely different between tumors and radiation injury.

Our results are consistent with published clinical brain tumor MTR data (19-21), where the effects of increased intratumoral fluid (decreased MTR) apparently dominate those of increased cellularity (increased MTR). We are not aware of clinical reports on the use of MTR in radiation injury. However, our results (decreased MTR) are consistent with what would be expected due to edema and loss of cellularity. The contrasting ADC patterns we observe for radiation injury (increased ADC) and tumor (decreased ADC) have significant potential in the clinical scenario, and match clinical observations for each pathology alone (6,16-18). We suspect that, as in Figures 4 and 5, the presence of both recurrent tumor and radiation injury results in a mixed-contrast ADC map, in which active tumor appears hypointense and radiation injury hyperintense relative to healthy tissue.

The mixed tumor/radiation necrosis case typically observed clinically is more complicated than is represented in our irradiated glioma model. However, this does not detract from the significance of our work as a first step toward a mixed injury model. While our long-term goal is to generate and characterize an animal model that presents both tumor recurrence and radiation injury to normal brain tissue, the production of such a model is not simple. In this work, we chose the lowest radiation dose that would ensure an increase in survival, as shown in **Supplementary Figure 2**, but still allow tumor re-growth. Determining the ideal radiation dose to generate concurrent tumor recurrence and radiation injury to normal tissue is a challenging next step, as higher doses of radiation increase the likelihood of completely eliminating the tumor. An alternative approach to generating a mixed tumor/necrosis model is to implant the tumor cells into irradiated brains. Once a more mature mixed model of tumor recurrence and necrosis has been developed and validated, diffusion, magnetization transfer, and other imaging modalities can all be applied to help address the challenging clinical problem of discriminating necrosis and tumor.

Supplementary Material

Refer to Web version on PubMed Central for supplementary material.

Acknowledgments

This project has been supported by NIH grant R01 CA155365 (JRG), and funding from the Alvin J. Siteman Comprehensive Cancer Center (P30), P30 CA091842, the Barnes-Jewish Hospital Foundation Cancer Frontier Fund, Mallinckrodt Institute of Radiology, and Elekta Instruments AB (Stockholm, Sweden).

References

1. Becker KP, Yu J. Status quo--standard-of-care medical and radiation therapy for glioblastoma. Cancer J. 2012; 18:12–19. [PubMed: 22290252]

2. Stupp R, Hegi ME, Mason WP, et al. Effects of radiotherapy with concomitant and adjuvant temozolomide versus radiotherapy alone on survival in glioblastoma in a randomised phase III study: 5-year analysis of the EORTC NCIC trial. Lancet Oncol. 2009; 10:459–466. [PubMed: 19269895]
3. Stupp R, Mason WP, van den Bent MJ, et al. Radiotherapy plus concomitant and adjuvant temozolomide for glioblastoma. N Engl J Med. 2005; 352:987–996. [PubMed: 15758009]
4. Kumar AJ, Leeds NE, Fuller GN, et al. Malignant Gliomas: MR Imaging Spectrum of Radiation Therapy- and Chemotherapy-induced Necrosis of the Brain after Treatment1. Radiology. 2000; 217:377–384. [PubMed: 11058631]
5. Eyster EF, Nielsen SL, Sheline GE, et al. Cerebral radiation necrosis simulating a brain tumor. Case report. J Neurosurg. 1974; 40:267–271. [PubMed: 4203210]
6. Shah R, Vattoth S, Jacob R, et al. Radiation necrosis in the brain: imaging features and differentiation from tumor recurrence. Radiographics. 2012; 32:1343–1359. [PubMed: 22977022]
7. Shah AH, Snelling B, Bregy A, et al. Discriminating radiation necrosis from tumor progression in gliomas: a systematic review what is the best imaging modality? Journal of Neuro-Oncology. 2013; 112:141–152. [PubMed: 23344789]
8. Stockham AL, Tievsky AL, Koyfman SA, et al. Conventional MRI does not reliably distinguish radiation necrosis from tumor recurrence after stereotactic radiosurgery. Journal of Neuro-Oncology. 2012; 109:149–158. [PubMed: 22638727]
9. Greene-Schloesser D, Robbins ME, Peiffer AM, et al. Radiation-induced brain injury: A review. Frontiers in Oncology. 2012; 2:73. [PubMed: 22833841]
10. Rahmathulla G, Marko NF, Weil RJ. Cerebral radiation necrosis: a review of the pathobiology, diagnosis and management considerations. J Clin Neurosci. 2013; 20:485–502. [PubMed: 23416129]
11. Siu A, Wind JJ, Iorgulescu JB, et al. Radiation necrosis following treatment of high grade glioma--a review of the literature and current understanding. Acta Neurochir (Wien). 2012; 154:191–201. discussion 201. [PubMed: 22130634]
12. Wong CS, Van der Kogel AJ. Mechanisms of radiation injury to the central nervous system: implications for neuroprotection. Mol Interv. 2004; 4:273–284. [PubMed: 15471910]
13. Calvar JA, Meli FJ, Romero C, et al. Characterization of brain tumors by MRS, DWI and Ki-67 labeling index. Journal of Neuro-Oncology. 2005; 72:273–280. [PubMed: 15937653]
14. Choi SY, Chang YW, Park HJ, et al. Correlation of the apparent diffusion coefficiency values on diffusion-weighted imaging with prognostic factors for breast cancer. Br J Radiol. 2012; 85:e474–479. [PubMed: 22128125]
15. Wang Y, Chen ZE, Yaghmai V, et al. Diffusion-weighted MR imaging in pancreatic endocrine tumors correlated with histopathologic characteristics. J Magn Reson Imaging. 2011; 33:1071–1079. [PubMed: 21509863]
16. Gauvain KM, McKinstry RC, Mukherjee P, et al. Evaluating pediatric brain tumor cellularity with diffusion-tensor imaging. AJR Am J Roentgenol. 2001; 177:449–454. [PubMed: 11461881]
17. Gupta RK, Cloughesy TF, Sinha U, et al. Relationships between choline magnetic resonance spectroscopy, apparent diffusion coefficient and quantitative histopathology in human glioma. Journal of Neuro-Oncology. 2000; 50:215–226. [PubMed: 11263501]
18. Sugahara T, Korogi Y, Kochi M, et al. Usefulness of diffusion-weighted MRI with echo-planar technique in the evaluation of cellularity in gliomas. J Magn Reson Imaging. 1999; 9:53–60. [PubMed: 10030650]
19. Okumura A, Takenaka K, Nishimura Y, et al. The characterization of human brain tumor using magnetization transfer technique in magnetic resonance imaging. Neurological research. 1999; 21:250–254. [PubMed: 10319332]
20. Kurki T, Lundbom N, Kalimo H, et al. MR classification of brain gliomas: value of magnetization transfer and conventional imaging. Magn Reson Imaging. 1995; 13:501–511. [PubMed: 7674845]
21. Pui MH. Magnetization transfer analysis of brain tumor, infection, and infarction. J Magn Reson Imaging. 2000; 12:395–399. [PubMed: 10992306]
22. Jiang X, Perez-Torres CJ, Thotala D, et al. A GSK-3β inhibitor protects against radiation necrosis in mouse brain. Int J Radiat Oncol Biol Phys. 2014; 89:714–721. [PubMed: 24969790]

23. Jiang X, Engelbach J, Yuan L, et al. Anti-VEGF antibodies mitigate the development of radiation necrosis in mouse brain. Clin Cancer Res. 2014; 20:2695–2702. [PubMed: 24647570]
24. Kumanishi T. Brain tumors induced with Rous sarcoma virus, Schmidt-Ruppin strain. I. Induction of brain tumors in adult mice with Rous chicken sarcoma cells. Jpn J Exp Med. 1967; 37:461–474. [PubMed: 4301953]
25. Sherburn EW, Wanebo JE, Kim P, et al. Gliomas in rodent whisker barrel cortex: a new tumor model. J Neurosurg. 1999; 91:814–821. [PubMed: 10541239]
26. Barajas RF Jr. Chang JS, Segal MR, et al. Differentiation of recurrent glioblastoma multiforme from radiation necrosis after external beam radiation therapy with dynamic susceptibility-weighted contrast-enhanced perfusion MR imaging. Radiology. 2009; 253:486–496. [PubMed: 19789240]
27. Jain R, Narang J, Schultz L, et al. Permeability estimates in histopathology-proved treatment-induced necrosis using perfusion CT: can these add to other perfusion parameters in differentiating from recurrent/progressive tumors? AJNR Am J Neuroradiol. 2011; 32:658–663. [PubMed: 21330392]
28. Ozsunar Y, Mullins ME, Kwong K, et al. Glioma recurrence versus radiation necrosis? A pilot comparison of arterial spin-labeled, dynamic susceptibility contrast enhanced MRI, and FDG-PET imaging. Acad Radiol. 2010; 17:282–290. [PubMed: 20060750]
29. Amin A, Moustafa H, Ahmed E, et al. Glioma residual or recurrence versus radiation necrosis: accuracy of pentavalent technetium-99m-dimercaptosuccinic acid [Tc-99m (V) DMSA] brain SPECT compared to proton magnetic resonance spectroscopy (1H-MRS): initial results. Journal of Neuro-Oncology. 2012; 106:579–587. [PubMed: 21912937]
30. Zeng QS, Li CF, Liu H, et al. Distinction between recurrent glioma and radiation injury using magnetic resonance spectroscopy in combination with diffusion-weighted imaging. Int J Radiat Oncol Biol Phys. 2007; 68:151–158. [PubMed: 17289287]
31. Wang S, Tryggestad E, Zhou T, et al. Assessment of MRI parameters as imaging biomarkers for radiation necrosis in the rat brain. Int J Radiat Oncol Biol Phys. 2012; 83:e431–436. [PubMed: 22483739]
32. Goldman M, Boxerman JL, Rogg JM, et al. Utility of apparent diffusion coefficient in predicting the outcome of Gamma Knife-treated brain metastases prior to changes in tumor volume: a preliminary study. J Neurosurg. 2006; 105(Suppl):175–182. [PubMed: 18503353]

Summary

A major unmet challenge in the treatment of brain tumors is non-invasively differentiating recurrent tumor from delayed radiation injury. Herein, two MR protocols widely employed in the clinic, diffusion weighted imaging (DWI) and magnetization transfer contrast (MTC), are applied to mouse glioma and radiation injury models. Findings suggest that DWI may help discriminate between tumor and radiation effects while MTC, though incapable of such discrimination, is more sensitive to the presence of pathology.

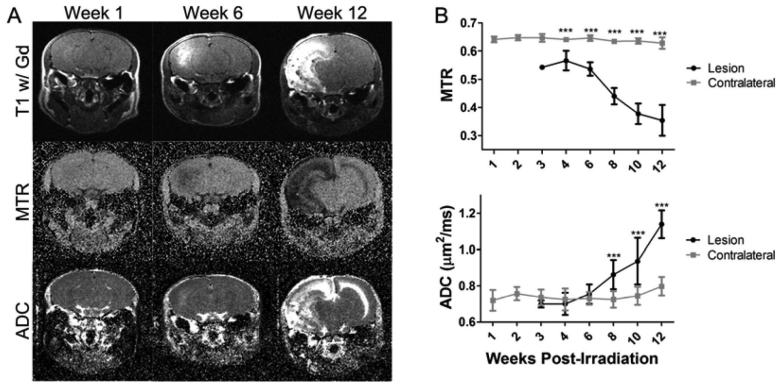

Figure 1.

MTR decreases and ADC increases in the radiation injury model. Panel **A** presents the post-contrast T1-weighted images (top), MTR maps (middle), and ADC maps (bottom) of a representative mouse at 1 (left), 6 (center), and 12 (right) weeks post-irradiation. The radiation lesion is bright on post-contrast T1. Panel **B** presents the group average MTR (top) and ADC (bottom) for the lesion and contralateral ROIs at all time points measured (mean ± SD, N=7). *** indicates P<0.001 as measured by Two-Way Repeated-Measures ANOVA with a Bonferroni post-test.

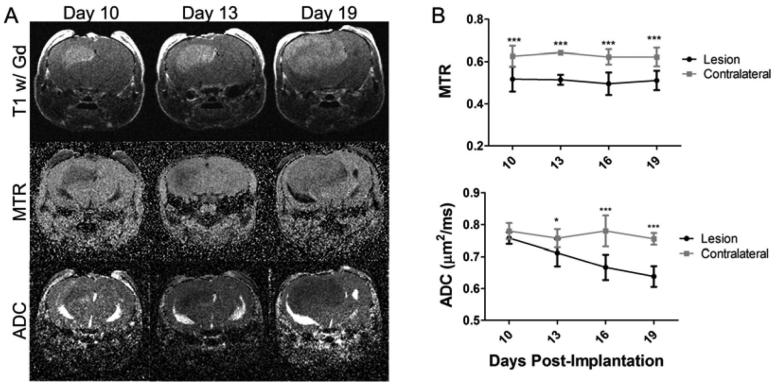

Figure 2.

MTR is consistently lower in tumors, while ADC decreases with tumor progression in the glioma model. Panel **A** presents the post-contrast T1-weighted images (top), MTR maps (middle), and ADC maps (bottom) of a representative mouse at PImD 10 (left), 13 (center), and 19 (right). The glioma is bright on post-contrast T1. Panel **B** presents the group average MTR (top) and ADC (bottom) for the lesion and contralateral ROIs at all time points measured (mean ± SD, N=10). * indicates $P<0.05$ and *** indicates $P<0.001$ as measured by Two-Way Repeated-Measures ANOVA with a Bonferroni post-test.

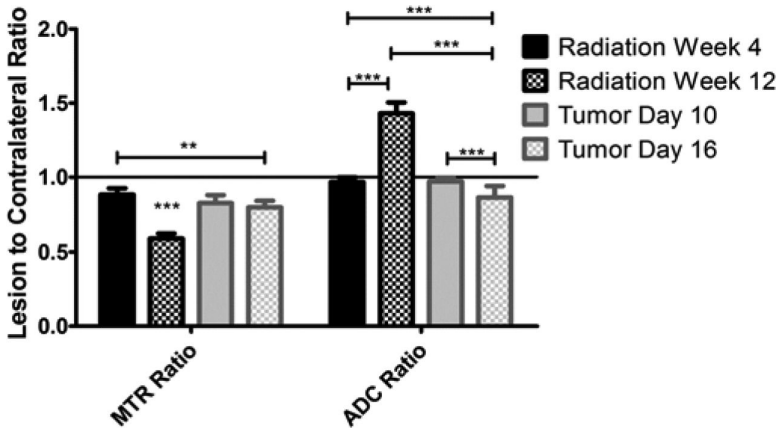

Figure 3.

ADC is better at differentiating tumor from radiation injury than MTR. For both metrics, the ratio of the lesion value to that in the contralateral hemisphere was calculated at both an early and a late development time point. MTR was significantly different for the late radiation injury time point compared with all others and for late tumor compared with early radiation injury. ADC was significant in all comparisons, except when both radiation and glioma were at the early time point. ** indicates P<0.01 and *** indicates P<0.001 as measured by Two-Way Repeated-Measures ANOVA with a Bonferroni post-test.

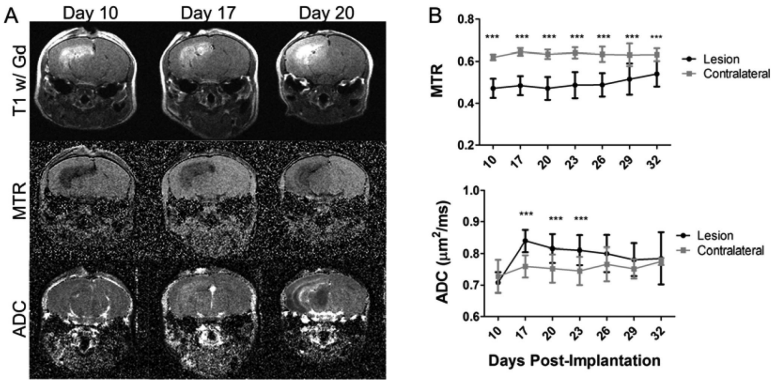

Figure 4.

MTR is consistently lower, while ADC is transiently increased in the irradiated glioma model. Panel **A** presents the post-contrast T1-weighted images (top), MTR maps (middle), and ADC maps (bottom) of a representative mouse at PImD 10 (left), 17 (center), and final (right). The lesion is bright on post-contrast T1. Panel **B** presents the group average MTR (top) and ADC (bottom) for the lesion and contralateral ROIs at all time points measured (mean ± SD, N=10). *** indicates P<0.001 as measured by Two-Way Repeated-Measures ANOVA with a Bonferroni post-test.

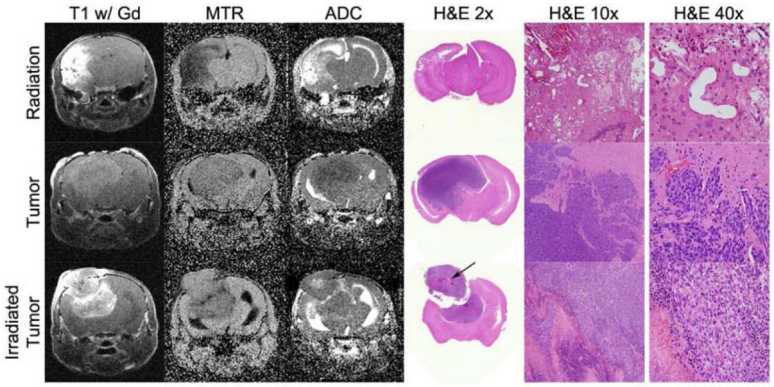

Figure 5.

Histology compared to the MRI metrics at the final time point. The top row presents a radiation injury example, the middle row presents an untreated glioma example, and the bottom row presents an irradiated glioma example. From left to right, columns show T1-weighted images, MTR maps, and ADC maps of the same slice followed by H&E-stained tissue slices at a comparable anatomical location at 2x, 10x and 40x magnification. The data shown in this figure are for different animals than those of Figures 1, 2, and 4. Of note, the H&E of the irradiated tumor confirms that there is a necrotic section within the tumor (arrow), consistent with the corresponding ADC map.